COOPERATIVE EFFECTS IN MODELS OF STEADY-STATE TRANSPORT ACROSS MEMBRANES

IV. ONE-SITE, TWO-SITE, AND MULTISITE MODELS

TERRELL L. HILL *and* YI-DER CHEN

From the Division of Natural Sciences, University of California, Santa Cruz, California 95060. Dr. Hill's present address is the Laboratory of Molecular Biology, National Institute of Arthritis and Metabolic Diseases, National Institutes of Health, Bethesda, Maryland 20014.

ABSTRACT Several different one-site, two-site, and multisite models of steady-state ion transport across a membrane are investigated. The basic features, including cooperative interactions between channels, are the same as in earlier papers in this series. In particular, the present paper represents a considerable elaboration of part III. The models might apply to artificial or possibly to biological membranes, but particular applications must await further elucidation of the molecular structure and operation of these membranes.

1. INTRODUCTION

This work is a continuation of three earlier papers (1–3) on the same general topic. We shall make use of notation and concepts introduced earlier without repeating details here. In particular, part III (3) is a preliminary version of the present paper.

Our original motivation in this work was possible application to K^+ transport across the nerve membrane. We now think this particular application is extremely unlikely, and we are presently working on a rather different nerve model.[1] However, because the models studied here are so basic and elementary, and because other authors (4–6)[2] believe that cooperativity *between* channels—as in the present models—is an essential feature of excitable membranes, the analysis here may well have eventual applications to or usefulness for some artificial and/or biological membranes.

---

[1] Hill, T. L. 1971. *In* Perspectives in Membrane Biophysics. D. Agin, editor. Gordon & Breach, Science Publishers, Inc., New York. In press. See also T. L. Hill and Y. Chen. 1971. *Proc. Nat. Acad. Sci. U. S. A.* Published in August 1971.

[2] Starzak, M. To be published.

Because of present uncertainty about the structure and molecular operation of biological membranes, it seems judicious to consider a variety of theoretical approaches, including this one which involves ion transport via binding on sites in the membrane. As will be seen below, these models, except in very special cases, lead to nonlinear steady-state flux-potential curves for a "pure" conformation. However, it is in part for this reason that application to the squid membrane, at least, seems very unlikely,[1] for the corresponding experimental ("instantaneous") curves are approximately linear, for both K^+ and Na^+.

Some of the paper (sections 3–5) will be concerned with models in which each unit of the membrane can exist in two different conformations, as in our earlier work (1, 3). However, as a necessary prerequisite, attention is also given to one-conformation models (section 2). Section 6 is concerned with one-conformation, multisite models.

2. SIMPLE ONE-CONFORMATION MODELS

We present in this section a partial "catalogue" of flux-potential curves for simple one-site and two-site models. We limit the examples chosen in sections 2 A and 2 B to the special case of equal ionic concentration in the baths (on either side of the membrane). However, cases in which these concentrations differ are illustrated in sections 2 C, 3, and 5. We shall refer here to the ion being transported as M^+ (rather than K^+).

A. One-Site Model

Fig. 1 shows the model we consider first. The single binding site for M^+ in each unit is located at an arbitrary position y in the membrane ($y = 0.50$ in part III), where the

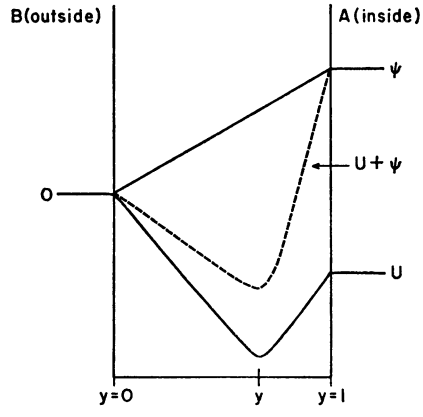

FIGURE 1

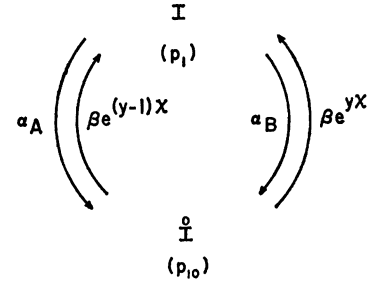

FIGURE 2

FIGURE 1 Variation of electrostatic potential ψ and binding potential energy U across membrane. Binding site is at y.

FIGURE 2 States and rate constants for a membrane unit with site at y.

electrostatic potential is $y\psi$. The assumed adsorption and desorption rate constants are indicated in Fig. 2. Then the fractions of units in each of the two states, at steady state, are

$$p_1 = \beta e^{yx}(1 + e^{-x})/\sum \quad \text{and} \quad p_{10} = (\alpha_A + \alpha_B)/\sum, \tag{1}$$

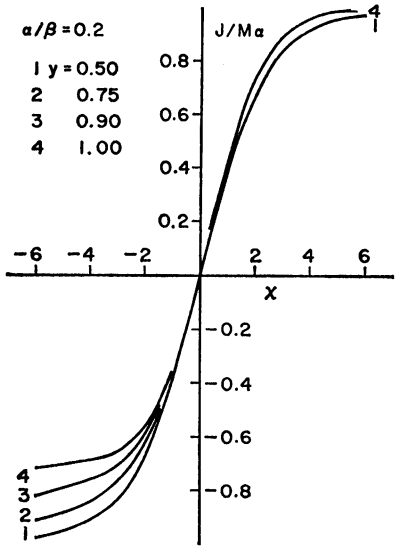

FIGURE 3

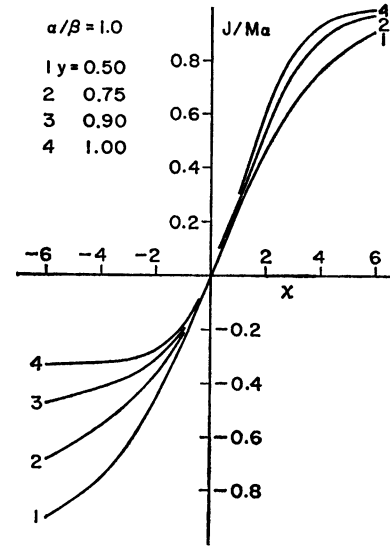

FIGURE 4

FIGURES 3 and 4 Ionic flux as a function of membrane potential ($\alpha_A = \alpha_B = \alpha$).

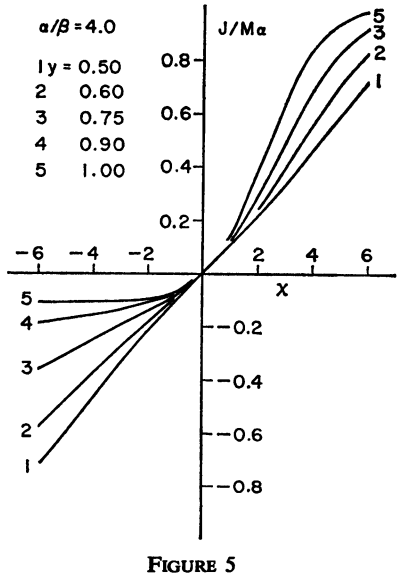

FIGURE 5

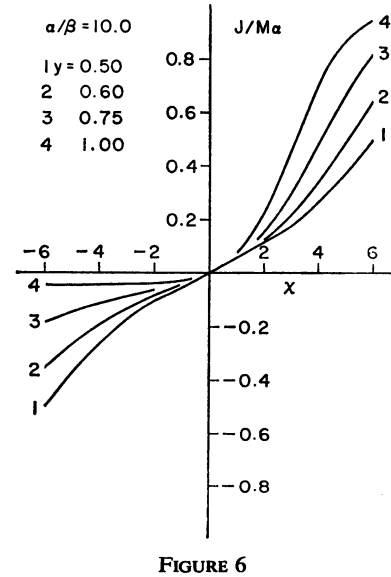

FIGURE 6

FIGURES 5 and 6 Ionic flux as a function of membrane potential ($\alpha_A = \alpha_B = \alpha$).

where $x = e\psi/kT (x = 1 \leftrightarrow \psi \cong 25$ mv) and

$$\sum = \alpha_A + \alpha_B + \beta e^{yx}(1 + e^{-x}). \tag{2}$$

The flux $(A \rightarrow B)$ for a membrane with M units is

$$J = M\beta e^{yx}(\alpha_A - \alpha_B e^{-x})/\sum. \tag{3}$$

Figs. 3–6 show the dependence of $J/M\alpha$ on x, all in the special case $\alpha_A = \alpha_B = \alpha$, for various values of α/β and y. Because of the symmetry of the model, it suffices to consider the range $0.50 \leq y \leq 1$. J is an odd function of x when $y = 0.50$. There is considerable variety in these curves, even with such a simple model.

B. Two-Site Model

A two-site version of the above model is shown in Fig. 7. The maximum between the two minima in the potential curve U is assumed for simplicity to be located at $(y_A + y_B)/2$. The rate constants and notation for the four states are indicated in Fig. 8, where

$$\beta'_A = \beta_A r s_A^2, \quad \beta'_B = \beta_B s_B^2, \quad \kappa'_A = \kappa_A s_A/s_B, \quad \kappa'_B = \kappa_B s_B/s_A,$$

$$s_A = e^{y_A x/2}, \quad s_B = e^{y_B x/2}, \quad r = e^{-x}. \tag{4}$$

As usual, we have employed simple transition-state rate theory in making these assignments. The β's and κ's are not all independent; detailed balance requires that $\beta_B \kappa_A = \beta_A \kappa_B$.

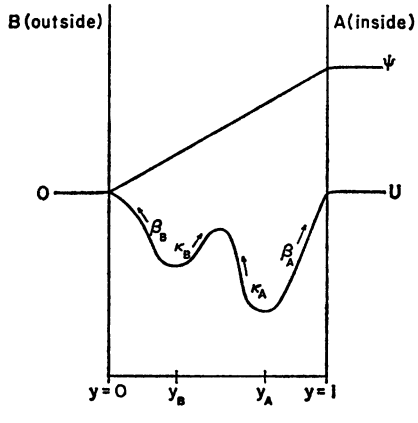

FIGURE 7

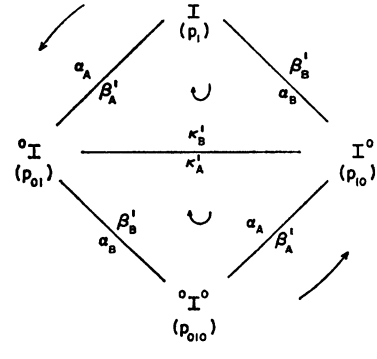

FIGURE 8

FIGURE 7 Variation of electrostatic potential ψ and binding potential energy U across membrane. Binding sites are at y_A and y_B.

FIGURE 8 States and rate constants for a membrane unit with sites at y_A and y_B. See also equations 4.

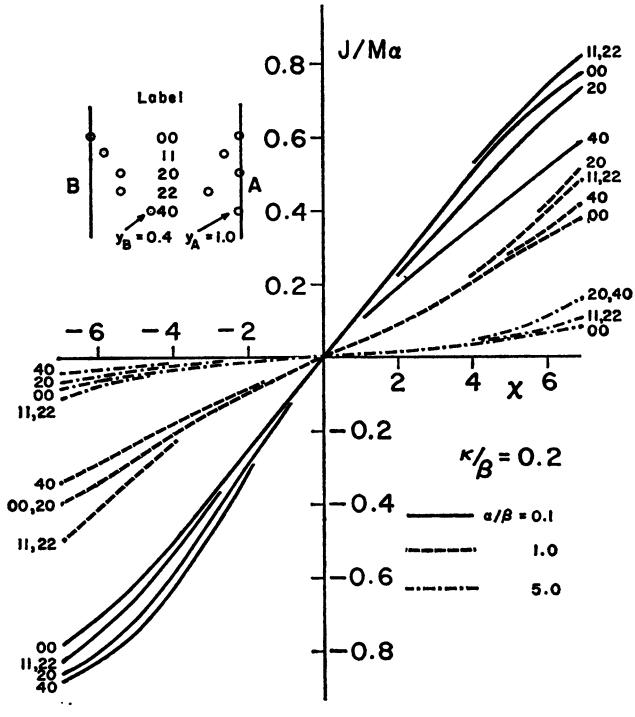

FIGURE 9 Ionic flux as a function of membrane potential ($\alpha_A = \alpha_B = \alpha$). The labels on the curves indicate the location of sites, as shown in the inset.

The steady-state probabilities of the four states are easily found to be (7, 8)

$$p_1 = [\beta'_A\beta'_B(\alpha_A + \alpha_B + \beta'_A + \beta'_B) + (\beta'_A + \beta'_B)(\kappa'_A\beta'_B + \kappa'_B\beta'_A)]/\sum, \quad (5)$$

$$p_{01} = [\alpha_A\beta'_B(\alpha_A + \alpha_B + \beta'_A + \beta'_B) + \kappa'_B(\alpha_A + \alpha_B)(\beta'_A + \beta'_B)]/\sum, \quad (6)$$

$$p_{10} = [\alpha_B\beta'_A(\alpha_A + \alpha_B + \beta'_A + \beta'_B) + \kappa'_A(\alpha_A + \alpha_B)(\beta'_A + \beta'_B)]/\sum, \quad (7)$$

$$p_{010} = [\alpha_A\alpha_B(\alpha_A + \alpha_B + \beta'_A + \beta'_B) + (\alpha_A + \alpha_B)(\kappa'_A\alpha_A + \kappa'_B\alpha_B)]/\sum, \quad (8)$$

where

$$\sum = (\alpha_A + \alpha_B + \beta'_A + \beta'_B)[(\alpha_A + \beta'_A)(\alpha_B + \beta'_B) + \kappa'_A\beta'_B + \kappa'_B\beta'_A] + (\alpha_A + \alpha_B)[\kappa'_A(\alpha_A + \beta'_A) + \kappa'_B(\alpha_B + \beta'_B)]. \quad (9)$$

The steady-state flux is

$$J = M(\alpha_A + \alpha_B + \beta'_A + \beta'_B)(\alpha_A\kappa'_A\beta'_B - \alpha_B\kappa'_B\beta'_A)/\sum. \quad (10)$$

At equilibrium, $\alpha_A = \alpha_B e^{-x}$ and $J = 0$.

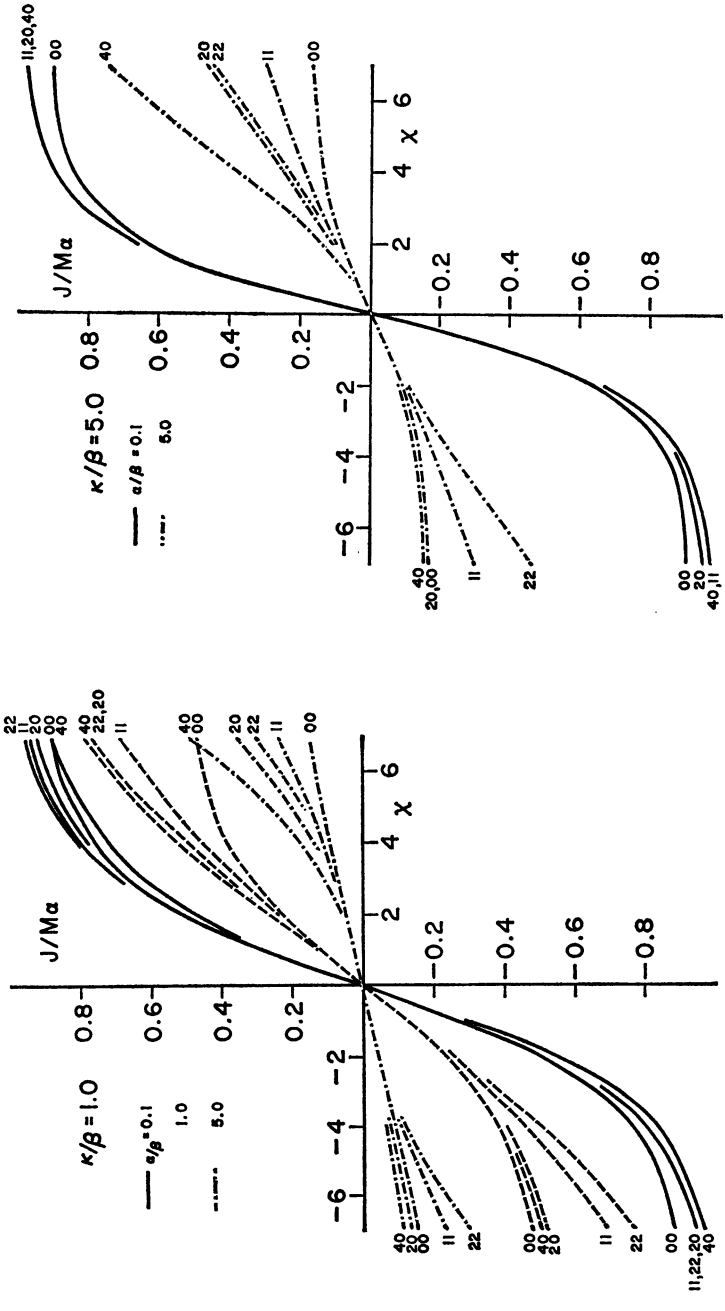

FIGURE 10

FIGURE 11

FIGURES 10 and 11 Ionic flux as a function of membrane potential ($\alpha_A = \alpha_B = \alpha$). For meaning of labels on curves, see Fig. 9.

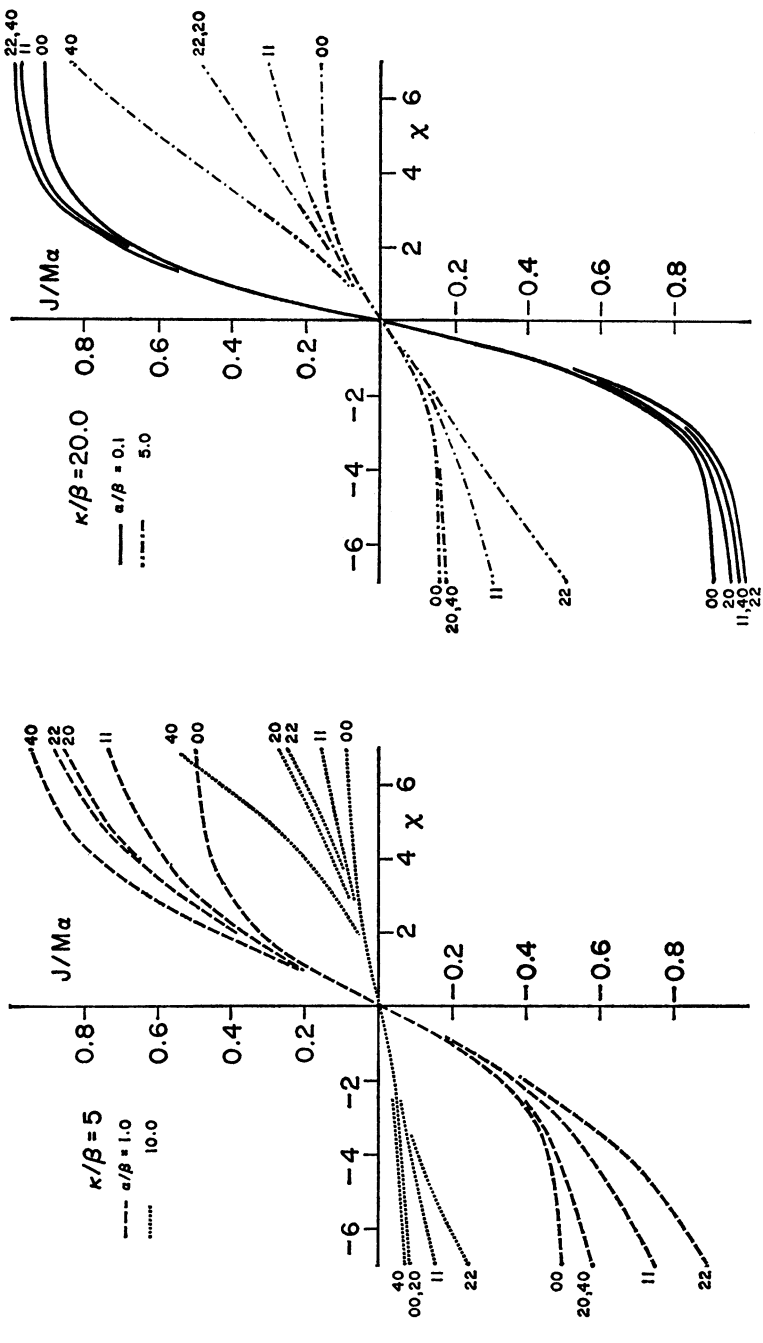

FIGURE 12

FIGURE 13

FIGURES 12 and 13 Ionic flux as a function of membrane potential ($\alpha_A = \alpha_B = \alpha$). For meaning of labels on curves, see Fig. 9.

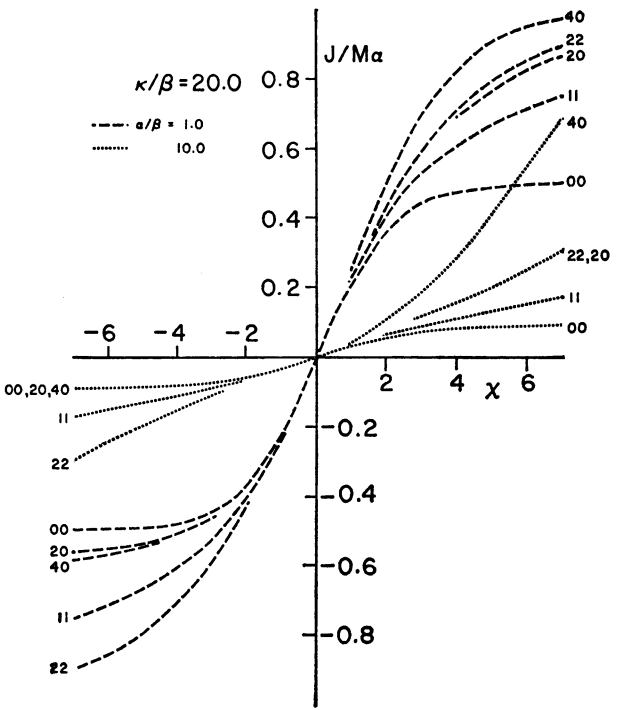

FIGURE 14

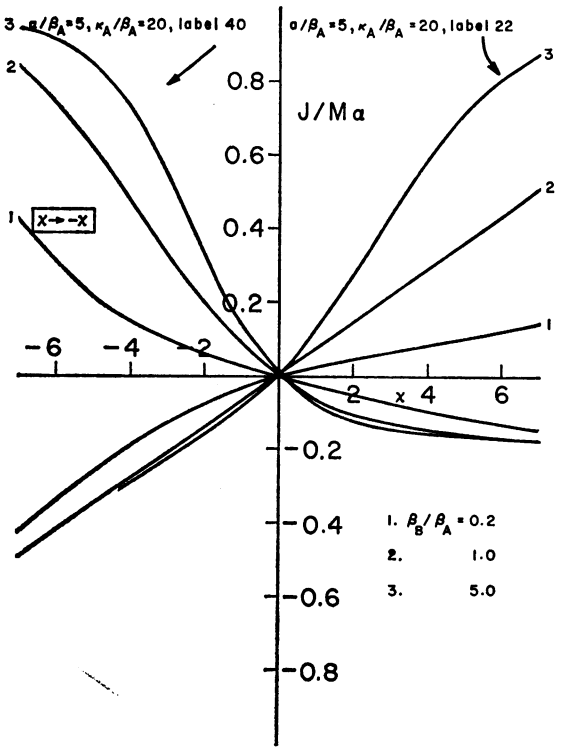

FIGURE 15

FIGURE 14 Ionic flux as a function of membrane potential ($\alpha_A = \alpha_B = \alpha$). For meaning of labels on curves, see Fig. 9.

FIGURE 15 Ionic flux as a function of membrane potential ($\alpha_A = \alpha_B = \alpha$). Cases with $\beta_A \neq \beta_B$. The three curves indicated by $x \rightarrow -x$ have the x-axis reversed in direction (to accommodate more curves in the figure).

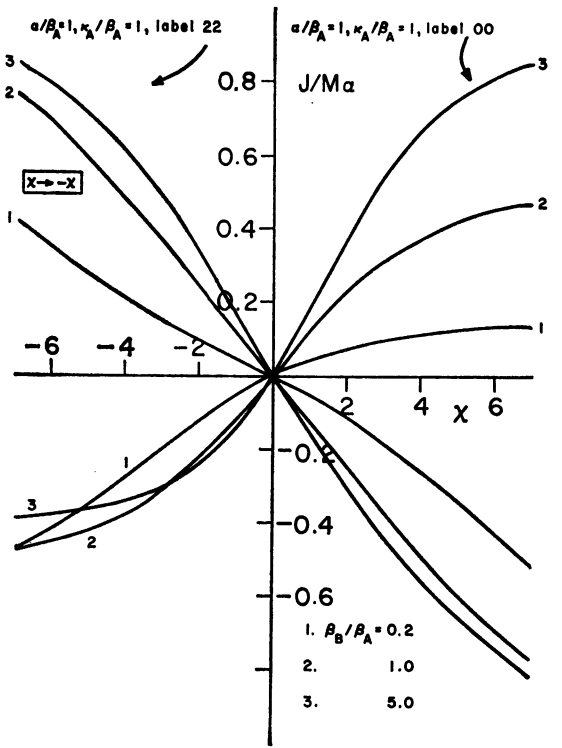

FIGURE 16

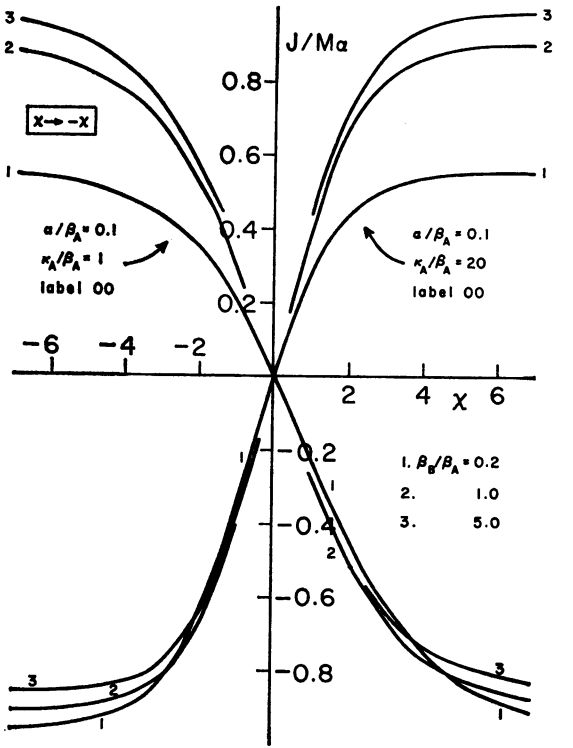

FIGURE 17

FIGURES 16 and 17 Ionic flux as a function of membrane potential ($\alpha_A = \alpha_B = \alpha$). Cases with $\beta_A \neq \beta_B$. The three curves indicated by $x \rightarrow -x$ have the x-axis reversed in direction (to accommodate more curves in the figure).

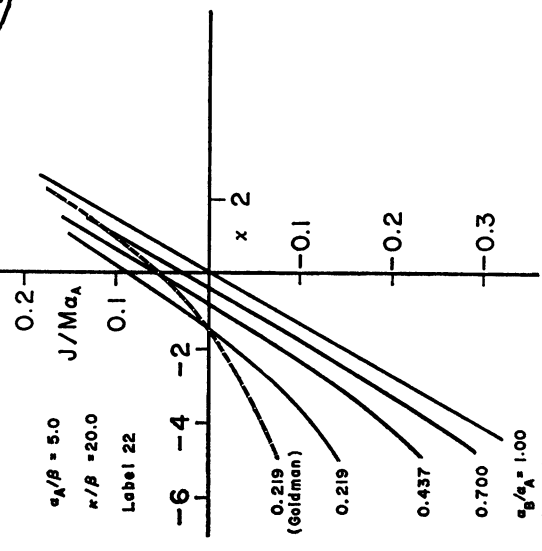

FIGURE 18

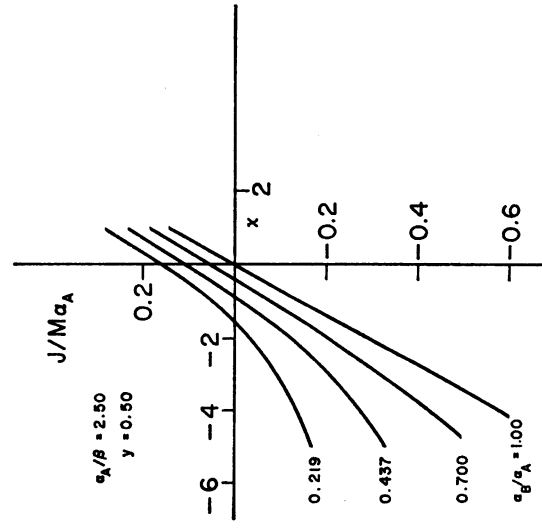

FIGURE 19

FIGURE 18 "One-site" theoretical flux-potential curves, in absence of conformational change.

FIGURE 19 "Two-site" theoretical flux-potential curves, in absence of conformational change. The dashed curve ($\alpha_B/\alpha_A = 0.219$) is from the Goldman equation (relative to the $\alpha_B/\alpha_A = 1.00$ line in the figure).

Figs. 9–14 illustrate the dependence of $J/M\alpha$ on x when $\alpha_A = \alpha_B = \alpha, \beta_A = \beta_B = \beta$, and $\kappa_A = \kappa_B = \kappa$. The remaining parameters are κ/β, α/β, y_A, and y_B. The shorthand labeling system used in these figures for y_A and y_B is included in Fig. 9. Curves with labels 00, 11, 22, etc., are odd functions of x. Also, a curve, say, for 04 is obvious (by symmetry) from 40, etc.

Figs. 15–17 present a few examples in which $\beta_A/\beta_B = \kappa_A/\kappa_B \neq 1$, though we still take $\alpha_A = \alpha_B = \alpha$. Recall (1) that a deep potential well (Fig. 7) is associated with strong binding and a small value of β. For example, in Fig. 7, $\beta_B > \beta_A$ and $\kappa_B > \kappa_A$. In effect, in each family of three curves in these figures, α, β_A, and κ_A are held constant, while β_B and κ_B are varied ($\kappa_B/\kappa_A = \beta_B/\beta_A$). The symmetry of the $J(x)$ curves (referred to in the preceding paragraph) is of course destroyed when $\beta_A \neq \beta_B$. It is apparent from these examples that asymmetry in the β's can more or less duplicate the effects of asymmetry in site locations (seen in Figs. 9–14). But, for simplicity, we confine ourselves in the remainder of this paper to cases in which $\beta_A = \beta_B$.

C. Examples with $\alpha_A \neq \alpha_B$

Some experimental results of Mozhayeva (9), and the well-known (10, 11) Goldman equation, both suggest that we might illustrate $\alpha_A \neq \alpha_B$ by choosing cases in which practically linear $J(x)$ curves are obtained when $\alpha_A = \alpha_B$. It is clear from Figs. 3–6 and 9–14 that, for *particular* parameter choices, simple one-site and two-site models do in fact lead to essentially linear curves. We have not made a study of the range of parameters giving this kind of behavior, but merely select here two arbitrary examples, suggested by the above figures. These "linear" examples are included in Figs. 18 (one-site; $\alpha/\beta = 2.5$, $y = 0.5$) and 19 (two-site; $\kappa/\beta = 20$, $\alpha/\beta = 5$, label 22), along with curves for $\alpha_B/\alpha_A \neq 1$. The Goldman equation is also illustrated in Fig. 19: the value of P (see below) is adjusted to make the linear ($\alpha_B/\alpha_A = 1.00$) Goldman curve coincide with the two-site linear curve; then, with this value of P, the $\alpha_B/\alpha_A = 0.219$ Goldman curve appears as the dashed line in the figure. Intermediate Goldman curves are omitted to avoid confusion.

The Goldman equation is usually derived (10, 11) from a continuum model, but we show in section 6 that, as one might expect, it is also a limiting form of the flux for a discrete-site model when the number of sites is large. In the notation of section 6, this equation can be written

$$J = MPx(\alpha_A e^x - \alpha_B)/(e^x - 1), \tag{11}$$

where P is a permeability coefficient.

3. ONE-SITE, TWO-CONFORMATION MODEL

We here generalize section 2 A to a model in which each unit may exist in one of two conformations, I and II, and each conformation has one binding site for M^+. The

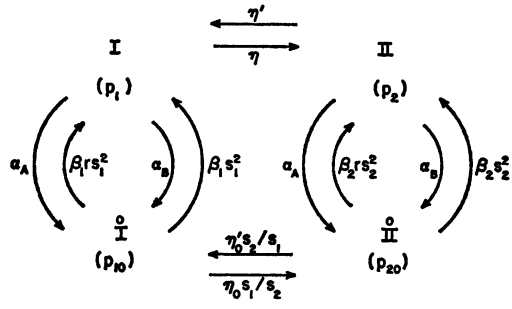

FIGURE 20 States and rate constants for a one-site, two-conformation membrane unit.

notation is a combination of that in sections 2 A and 2 B. In conformation I, the site is at y_1 ; in II, it is at y_2. In the transition state between conformations I and II, we assume the site to be located at $(y_1 + y_2)/2$. The diagram and rate constants are shown in Fig. 20 (see also Fig. 1 of part III [3]), where $s_i = e^{y_i x/2}$ and $r = e^{-x}$.

The present treatment is a generalization of part III in that the sites have arbitrary locations (y_1 and y_2) and we may have $\alpha_A \neq \alpha_B$.

The equilibrium grand partition function (g.p.f.) for one unit is the same as in equation III-7 except that the two $e^{-x/2}$ factors there are replaced by $e^{-y_1 x}$ and $e^{-y_2 x}$, respectively. Equations III-3, III-10, and III-11 all hold, as before.

After considerable algebra, the probabilities of the four states at steady state can be written

$$p_1 = (\eta' \beta_2 s_2^2 F)\beta_1 s_1^2 (1 + r)/\sum, \tag{12}$$

$$p_{10} = (\eta' \beta_2 s_2^2 F)(\alpha_A + \alpha_B)/\sum, \tag{13}$$

$$p_2 = (\eta \beta_1 s_1^2 F)\beta_2 s_2^2 (1 + r)/\sum, \tag{14}$$

$$p_{20} = (\eta \beta_1 s_1^2 F)(\alpha_A + \alpha_B)/\sum, \tag{15}$$

where

$$F = 1 + r + \frac{1}{s_1 s_2}\left[\frac{\eta_0}{\beta_1} + \frac{\eta_0'}{\beta_2} + \frac{\eta_0}{\beta_1 \eta}(\alpha_A + \alpha_B)\right], \tag{16}$$

$$\sum = \eta' \beta_2 s_2^2 F \sum_1 + \eta \beta_1 s_1^2 F \sum_2, \tag{17}$$

$$\sum_i = \alpha_A + \alpha_B + \beta_i s_i^2 (1 + r) \qquad (i = 1, 2). \tag{18}$$

Note that $\sum_i$ is the one-conformation $\sum$ of equation 2.

It is interesting that, in this one-site model, the inclusion of the other conformation in the steady state does not perturb the "internal" ratios p_1/p_{10} and p_2/p_{20} (compare equation 1 with equations 12–15). This is a quasi-equilibrium property which is not

maintained in models with two or more sites per conformation. However, in these more complicated models, this property can be made the basis of a useful approximation (section 4).

According to equations 12–15, the ratio of the two conformations at steady state is

$$\frac{P_2}{P_1} = \frac{p_2 + p_{20}}{p_1 + p_{10}} = \frac{\eta(\sum_2/\beta_2 s_2^2)}{\eta'(\sum_1/\beta_1 s_1^2)}. \tag{19}$$

Here, η/η' is an equilibrium property (equation III-11), and the other quantities on the right-hand side are *one*-conformation steady-state properties.

Four cycles contribute to the flux. The final expression for J is very simple:

$$J = P_1 J_1 + P_2 J_2, \tag{20}$$

where

$$J_i = M\beta_i s_i^2(\alpha_A - \alpha_B r)/\sum_i \qquad (i = 1, 2) \tag{21}$$

is the one-conformation flux (equation 3). The simple additivity in equation 20 is a reflection of the lack of perturbation of one conformation by the other, referred to above. Equation 20 does not hold exactly in models with more than one site per conformation.

We illustrate the application of equation 20 by a case similar to those in Figs. 3 and 4 of part III. We take:

$$\text{I:} \quad \alpha_A/\beta_1 = 4.0, \quad y_1 = 0.80,$$

$$\text{II:} \quad \alpha_A/\beta_2 = 0.30, \quad y_2 = 0.80.$$

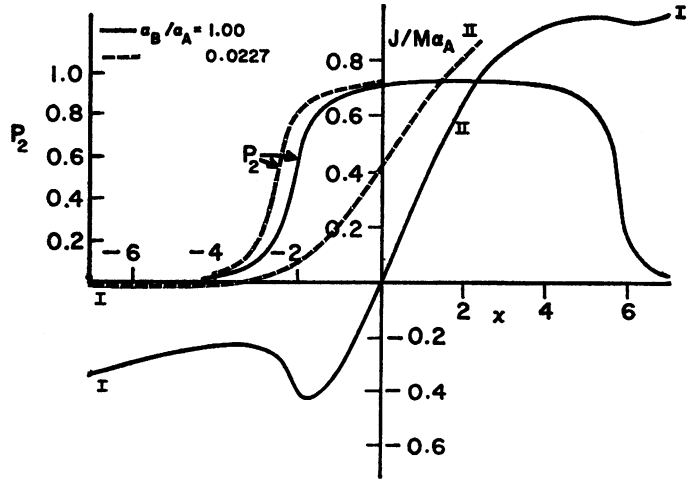

FIGURE 21 Illustration of model in Fig. 20.

Also, we use $Q = 0.0627$, $a = e^{1.60}$, $\delta = -0.32$, and $\gamma = 0.14$. Q was chosen to give $P_2 = 0.50$ (center of transition) at $x = -2.15$. A negative δ causes the transition to occur at larger $|x|$ for x positive than for x negative. Incidentally, a negative value of δ implies that the net (algebraic) charge on I is greater than that on II.

Fig. 21 shows the theoretical $J(x)$ for $\alpha_B/\alpha_A = 1.00$ ($M_e^+ = M_i^+$) and $\alpha_B/\alpha_A = 0.0227$ ($M_e^+ \ll M_i^+$). Theoretical $P_2(x)$ curves are included in the figure to show the conformational change.

4. QUASI-EQUILIBRIUM APPROXIMATION

We are, of course, already using the Bragg-Williams approximation (1) in our treatment of interactions between neighboring units. In this approximation the units may be considered "independent" despite the interactions. In this paper we take the Bragg-Williams approximation for granted, and are not referring to it, below, in our discussion of a quite different approximation.

The diagram method (7) of determining steady-state properties of a system of independent units is the method of choice when the diagram is not too complicated. Explicit analytical expressions for the p's and J may be derived, for example. If the diagram is quite complicated and a computer is available, the steady-state linear equations in the p's may be solved directly for each parameter set (see section 5). If the diagram is extremely complicated, a numerical Monte Carlo solution may be used (12).

In two-conformation models of intermediate complexity, where the one-conformation case is feasible but the two-conformation case is difficult, a quasi-equilibrium approximation may be useful. This approximation is suggested by the exact results of the preceding section.

The approximation consists of using equation 20 for J and an expression for P_2/P_1 which is based on the following analogy with the equilibrium situation. In the g.p.f. for an open system at equilibrium, the separate terms are proportional to the probability of observing the system in the corresponding states. Thus, in section 3,

$$\frac{P_2^e}{P_1^e} = \frac{\eta}{\eta'} \cdot \frac{(1 + q_2 \lambda_B e^{-\nu_2 x})}{(1 + q_1 \lambda_B e^{-\nu_1 x})} . \tag{22}$$

The factor η/η' (equation III-11) is equal to the probability ratio of conformations (p_2^e/p_1^e) with no ligand (M^+) bound; the two factors in parentheses provide a correction for the influence of bound ligand. In the steady-state approximation, we shall still use the equilibrium expression η/η' (which is correct at steady state in the model of section 3) for the ratio of "empty" conformation probabilities, but we need a generalization of the bound ligand effect. The parentheses themselves, in equation 22, are g.p.f.'s for binding. But "binding" g.p.f.'s are not defined at steady state. However, at equilibrium, a binding g.p.f. is equal to the reciprocal of the probability $P^e(0)$ that the system is empty (i.e., that there is no binding) (13, 14). Since $P(0)$ is

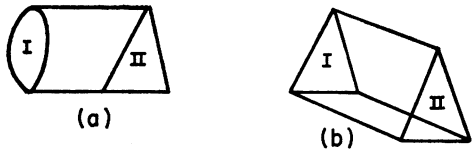

FIGURE 22 Two models used in study of quasi-equilibrium approximation.

a well defined quantity at steady state, as well as at equilibrium, we use $1/P(0)$ to construct the desired correction for ligand binding. That is we use, at steady state,

$$\frac{P_2}{P_1} = \frac{\eta}{\eta'} \cdot \frac{P_I(0)}{P_{II}(0)}, \tag{23}$$

where $P_I(0)$ is the one-conformation (I) steady-state probability that there is no binding, etc. The combination of equations 20 and 23 allows, then, the approximate calculation of steady-state properties of a two-conformation model from η/η' and exact steady-state one-conformation properties $[J_1, J_2, P_I(0), P_{II}(0)]$. The one-conformation properties may be found either from the diagram method or by direct numerical solution of the steady-state linear equations.

The approximation is exact in the special case of section 3. Thus, from equation 1,

$$P_I(0) = p_1 = \beta_1 s_1^2 (1 + r)/\sum_1 . \tag{24}$$

Hence equations 19 and 23 are identical in this case.

It should be emphasized that the "approximation" is really an approximation only under conditions such that both conformations are present in significant amounts (i.e., in the region of the conformational change). Otherwise, the approximation automatically gives the correct properties of the one conformation which virtually dominates. Actually, the latter situation prevails over most of the range in x in the two-conformation examples in this paper.

As a check, we have made a partial analytical study of the two models shown in Fig. 22 and have verified that equations 20 and 23 are not exact in these cases. Incidentally, Fig. 22 *a* has 16 flux diagrams (7) and 95 directional diagrams associated with it; Fig. 22 *b* has 50 flux diagrams and 450 directional diagrams. The diagram method is impractically complicated, or nearly so, in the latter case.

Also, in a numerical example (with $\alpha_A = \alpha_B$), related to Figs. 19 and 21, we compared exact results on Fig. 22 *b* (from the steady-state linear equations) with the approximation. The approximation was very effective: $J/M\alpha$ and P_2 were in error by at most 0.001 (usually by much less than this, especially in the case of P_2).

5. TWO-SITE, TWO-CONFORMATION MODEL

Here we extend section 2 B to a two-conformation model. We first present the necessary generalities, then an illustration.

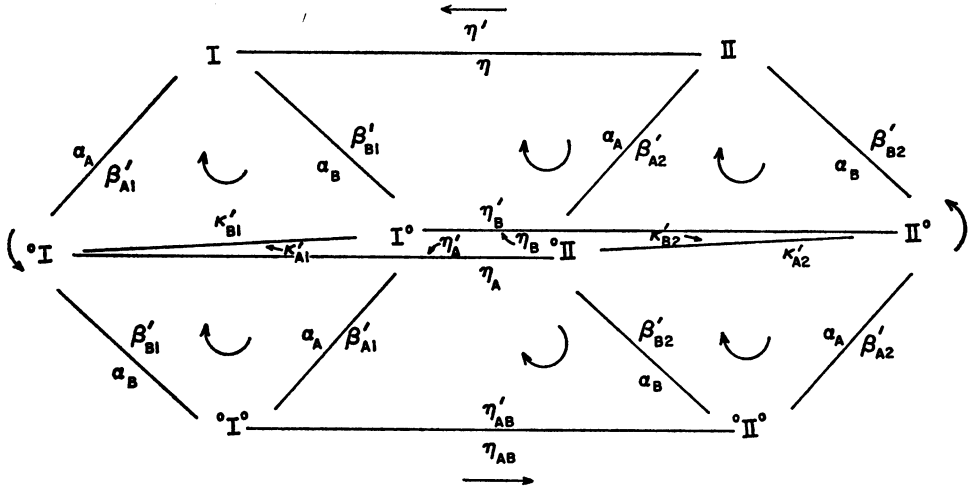

FIGURE 23 States and rate constants for a two-site, two-conformation membrane unit. See also equations 25–28.

Fig. 23 (see also Figs. 7 and 8) shows the diagram and rate constants, where

$$\beta'_{Ai} = \beta_{Ai} r s_{Ai}^2, \quad \beta'_{Bi} = \beta_{Bi} s_{Bi}^2, \quad \kappa'_{Ai} = \kappa_{Ai} s_{Ai}/s_{Bi}, \quad \kappa'_{Bi} = \kappa_{Bi} s_{Bi}/s_{Ai},$$
$$s_{Ai} = e^{\nu_{Ai} x/2}, \quad s_{Bi} = e^{\nu_{Bi} x/2}, \quad r = e^{-x} \qquad (i = 1, 2). \tag{25}$$

These are the same rate constants, for each conformation, as in equations 4. Detailed balance, at equilibrium, requires that

$$\beta_{A1}\kappa_{B1} = \beta_{B1}\kappa_{A1}, \quad \beta_{A2}\kappa_{B2} = \beta_{B2}\kappa_{A2},$$
$$\eta\beta'_{A1}\eta'_A = \eta'\beta'_{A2}\eta_A, \quad \eta\beta'_{B1}\eta'_B = \eta'\beta'_{B2}\eta_B,$$
$$\eta\beta'_{A1}\beta'_{B1}\eta'_{AB} = \eta'\beta'_{A2}\beta'_{B2}\eta_{AB}. \tag{26}$$

At equilibrium, $\alpha_B e^{-x} = \alpha_A$, as usual.

To proceed further, we need additional kinetic assumptions. For simplicity and in the absence of information to the contrary, we continue to assign to the transition state properties which are intermediate between those of reactant and product. Examples of this have already appeared in equations 4 and 25, and in Fig. 20. Other examples, which we employ here as well, were introduced in equations II-13 and II-14. In addition, we assume that the transition state has a polarizability and effective net charge intermediate between the values for conformations I and II. We then have

$$\eta = \eta(0) a^{P_2} e^{-\delta x/2} e^{-\gamma x^2/2},$$
$$\eta' = Q\eta(0) a^{P_1} e^{\delta x/2} e^{\gamma x^2/2}, \tag{27}$$

where $\eta(0)$, which we use as the reference rate constant (2), is the value of η when $w = 0$ and $x = 0$. Also,

$$\eta_A = \eta\left(\frac{\beta_{A1}}{\beta_{A2}}\right)^{1/2}\frac{s_{A1}}{s_{A2}}, \qquad \eta'_A = \eta'\left(\frac{\beta_{A2}}{\beta_{A1}}\right)^{1/2}\frac{s_{A2}}{s_{A1}},$$

$$\eta_B = \eta\left(\frac{\beta_{B1}}{\beta_{B2}}\right)^{1/2}\frac{s_{B1}}{s_{B2}}, \qquad \eta'_B = \eta'\left(\frac{\beta_{B2}}{\beta_{B1}}\right)^{1/2}\frac{s_{B2}}{s_{B1}},$$

$$\eta_{AB} = \eta\left(\frac{\beta_{A1}\beta_{B1}}{\beta_{A2}\beta_{B2}}\right)^{1/2}\frac{s_{A1}s_{B1}}{s_{A2}s_{B2}},$$

$$\eta'_{AB} = \eta'\left(\frac{\beta_{A2}\beta_{B2}}{\beta_{A1}\beta_{B1}}\right)^{1/2}\frac{s_{A2}s_{B2}}{s_{A1}s_{B1}}. \tag{28}$$

These relations are consistent with equations 26. In the illustration (below), to reduce the number of parameters, we restrict ourselves to the special case

$$\beta_{Ai} = \beta_{Bi} = \beta_i, \quad \kappa_{Ai} = \kappa_{Bi} = \kappa_i \qquad (i = 1, 2), \tag{29}$$

as in Figs. 9–14.

We have already illustrated the one-site model in Fig. 21. We repeat this process here, using the two-site model. We employ the steady-state linear equations rather than the diagram method (see section 4). We make the following choice of parameters:

$$\text{I:} \quad \alpha_A/\beta_1 = 5, \quad \kappa_1/\beta_1 = 5, \quad \text{label 40};$$

$$\text{II:} \quad \alpha_A/\beta_2 = 1, \quad \kappa_2/\beta_2 = 5, \quad \text{label 40}. \tag{30}$$

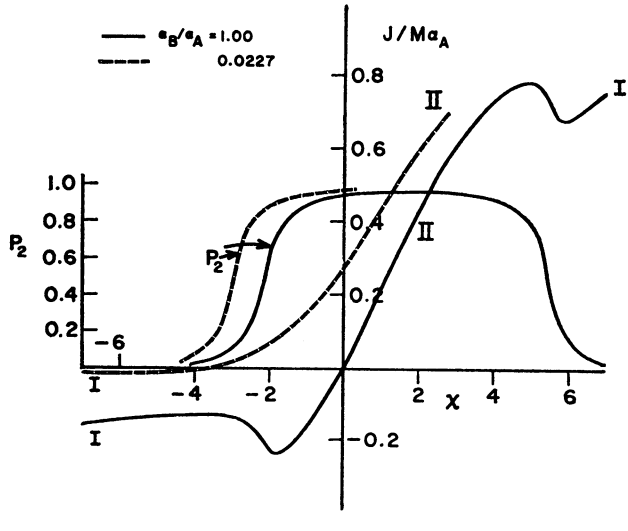

FIGURE 24 Illustration of model in Fig. 23. Compare Fig. 21.

We express rate constants and J/M in units of $\eta(0)$, and arbitrarily take (compare part II) $\beta_1 = 4\eta(0)$. That is,

$$\beta_1 = 4, \quad \alpha_A = 20, \quad \beta_2 = 20, \quad \kappa_1 = 20, \quad \kappa_2 = 100.$$

Also, we choose (see the end of section 3)

$$\delta = -0.30, \quad \gamma = 0.15, \quad a = e^{1.50}, \quad Q = 0.0248.$$

Equations 25, 27, and 28 then complete the assignment of rate constants required in Fig. 23. Fig. 24 (which is analogous to Fig. 21) shows the calculated flux curves for $\alpha_B/\alpha_A = 1.00$ and 0.0227. P_2 curves are also included in the figure.

6. MULTISITE, ONE-CONFORMATION MODELS

We first consider various cases of the model shown in Fig. 25. There are M independent channels of this sort in the membrane. The adsorption and desorption constants (for sites 0 and n) are α_A, α_B, and $\beta_A = \beta_B = \beta$. The κ's (Fig. 25) are rate constants for a jump between adjacent sites (the only kind of jump allowed). Ions in a channel do not interact with each other (except through the "exclusion principle": at most one ion per site).

A. Almost Empty Channel

In this case α_A/β and α_B/β are small so that the sites are almost always empty. Hence we can ignore the restriction that an ion cannot move into a site already occupied. Let $p_N \ll 1$ be the steady-state probability that the Nth site is occupied. Then

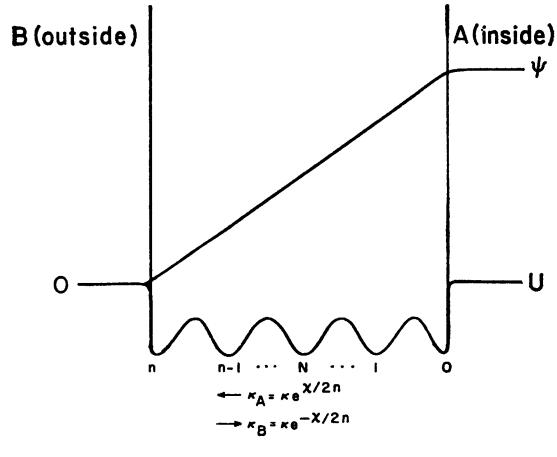

FIGURE 25 Multisite ionic transport model. Compare Fig. 7.

the steady-state linear equations are

$$0 = (\alpha_A - \beta p_0) + (\kappa_B p_1 - \kappa_A p_0)$$

$$0 = (\kappa_A p_0 - \kappa_B p_1) + (\kappa_B p_2 - \kappa_A p_1) \tag{31}$$

etc. The steady-state flux is

$$J/M = \alpha_A - \beta p_0 = \kappa_A p_0 - \kappa_B p_1 = \cdots . \tag{32}$$

If we use the method of Parlin and Eyring (15), we can combine equations 32 to eliminate the p's and find

$$\frac{J}{M} = \frac{\alpha_A e^x - \alpha_B}{e^x + 1 + [\beta(e^x - 1)/(\kappa_A - \kappa_B)]} . \tag{33}$$

When n is large, $\kappa_A - \kappa_B = \kappa x/n$. Then

$$\frac{J}{M} = \frac{\kappa x(\alpha_A e^x - \alpha_B)}{\beta n(e^x - 1)} \qquad (n \text{ large}). \tag{34}$$

This is the Goldman equation, 11, with permeability coefficient $P = \kappa/\beta n$. When $x = 0$, equation 33 becomes

$$J/M = \kappa(\alpha_A - \alpha_B)/(2\kappa + \beta n) \qquad (x = 0). \tag{35}$$

This agrees with equation 9 of Hill and Kedem (16), if, in that equation, we let α_A/β and α_B/β approach zero. Note that our $n + 1$ corresponds to their n.

Since the Goldman equation, 34, is of particular interest, we introduce another approach which is appropriate when n is large. The general (difference) equation of the set 31 can be rewritten as a differential equation in $p(N)$:

$$0 = -\frac{x}{n}\frac{\partial p}{\partial N} + \frac{\partial^2 p}{\partial N^2} \qquad (n \text{ large}). \tag{36}$$

The solution is

$$p(N) = c_1 e^{xN/n} + c_2 . \tag{37}$$

Because n is large, sites 0 and n will almost be in equilibrium with baths A and B, respectively, so that the boundary conditions are

$$p(0) = \alpha_A/\beta \quad \text{and} \quad p(n) = \alpha_B/\beta, \tag{38}$$

except for negligible terms. Then, from equations 37 and 38,

$$p(N) = \frac{(\alpha_B - \alpha_A)e^{xN/n} + \alpha_A e^x - \alpha_B}{\beta(e^x - 1)} . \tag{39}$$

To find the flux we use the second of equations 32:

$$\frac{J}{M} = \kappa_A p(0) - \kappa_B p(1) = (\kappa_A - \kappa_B)p(0) - \kappa\left(\frac{\partial p}{\partial N}\right)_{N=0}, \tag{40}$$

which leads again to equation 34. Note that, from the first of equations 32,

$$p(0) = \frac{\alpha_A}{\beta} - \frac{J}{M\beta}. \tag{41}$$

Hence the small terms dropped in equation 38 are $\pm J/M\beta$. These terms are smaller than the dominant terms by a factor of order $\kappa/n\beta$. Special cases of equations 34 and 39 are:

$$x = 0\text{: equation 35;} \qquad p(N) = \frac{\alpha_A}{\beta} + \frac{(\alpha_B - \alpha_A)(N/n)}{\beta}; \tag{42}$$

$$\int_0^n p(N)\, dN = n(\alpha_A + \alpha_B)/2\beta, \tag{43}$$

$$\alpha_A = \alpha_B: \frac{J}{M} = \left(\frac{\kappa x}{n}\right)\left(\frac{\alpha}{\beta}\right); \qquad p(N) = \frac{\alpha}{\beta}, \tag{44}$$

$$\alpha_A e^x = \alpha_B: J = 0; \quad p(N) = (\alpha_A/\beta)e^{xN/n}. \tag{45}$$

B. Almost Full Channel

In this case α_A/β and α_B/β are large. If we replace ions by "holes," this problem is essentially identical with the above. Let $p'_N \ll 1$ be the steady-state probability that the Nth site is empty. Then

$$\begin{aligned} 0 &= (\alpha_A p'_0 - \beta) + (\kappa_B p'_0 - \kappa_A p'_1) \\ 0 &= (\kappa_A p'_1 - \kappa_B p'_0) + (\kappa_B p'_1 - \kappa_A p'_2) \end{aligned} \tag{46}$$

etc. When n is large,

$$0 = \frac{x}{n}\frac{\partial p'}{\partial N} + \frac{\partial^2 p'}{\partial N^2}, \tag{47}$$

$$p'(N) = \frac{\beta[(\alpha_A - \alpha_B)e^{-xN/n} + \alpha_B e^{-x} - \alpha_A]}{\alpha_A \alpha_B (e^{-x} - 1)}, \tag{48}$$

$$\frac{J}{M} = \frac{\beta\kappa x(\alpha_A e^x - \alpha_B)}{\alpha_A \alpha_B n(e^x - 1)}. \tag{49}$$

Equation 49 is the flux in ions, not holes; it also has the form of a "Goldman equation." Equations 48 and 49 are identical with equations 39 and 34, respectively, if,

in the latter equations, we replace α_A/β, α_B/β, and N by β/α_B, β/α_A, and $n - N$, respectively.

C. Channel with Arbitrary Density

In this more general problem, "interference" between neighboring occupied sites has to be considered. The appropriate generalization of equations 31 and 46 is

$$0 = [\alpha_A(1 - p_0) - \beta p_0] + [\kappa_B p_1(1 - p_0) - \kappa_A p_0(1 - p_1)],$$

$$0 = [\kappa_A p_0(1 - p_1) - \kappa_B p_1(1 - p_0)] + [\kappa_B p_2(1 - p_1) - \kappa_A p_1(1 - p_2)], \quad (50)$$

etc. The flux J for $x = 0$ but arbitrary n is given by equation 9 of reference 16. We have not found a solution for arbitrary x and n.

The problem is not difficult when n is large (though numerical calculations are usually awkward). The differential equation is

$$0 = -\frac{x}{n}(1 - 2p)\frac{\partial p}{\partial N} + \frac{\partial^2 p}{\partial N^2}. \quad (51)$$

This can be written

$$\frac{\partial}{\partial N}\left[\frac{\partial p}{\partial N} - \frac{x}{n}(p - p^2)\right] = 0,$$

or

$$\frac{\partial p}{\partial N} - \frac{x}{n}(p - p^2) = c_1. \quad (52)$$

A second integration (with integration constant c_2) is then easy but the result, except in special cases, is a transcendental expression for $N(p)$. The boundary conditions, used to evaluate c_1 and c_2, are

$$p(0) = \frac{\alpha_A}{\alpha_A + \beta}, \qquad p(n) = \frac{\alpha_B}{\alpha_B + \beta}. \quad (53)$$

Using the method of equation 40, we find the flux to be

$$J/M = -\kappa c_1. \quad (54)$$

In the special case $x = 0$, we have

$$\frac{\partial^2 p}{\partial N^2} = 0, \qquad p(N) = \frac{\beta(\alpha_B - \alpha_A)(N/n)}{(\alpha_A + \beta)(\alpha_B + \beta)} + \frac{\alpha_A}{\alpha_A + \beta}, \quad (55)$$

$$\frac{J}{M} = \frac{\kappa\beta(\alpha_A - \alpha_B)}{n(\alpha_A + \beta)(\alpha_B + \beta)}. \quad (56)$$

Equation 56 is a special case of equation 9, reference 16.

When $\alpha_A = \alpha_B$, the differential equation is satisfied by

$$p = \frac{\alpha}{\alpha + \beta} = \text{constant.} \tag{57}$$

Then

$$J/M = -\kappa c_1 = (\kappa x/n)p(1 - p) = \kappa\alpha\beta x/n(\alpha + \beta)^2. \tag{58}$$

Note that J is linear in x.

In the general case (n large), a possibly useful interpolation formula for the flux is

$$\frac{J}{M} = \frac{\kappa\beta x(\alpha_A e^x - \alpha_B)}{n(\alpha_A + \beta)(\alpha_B + \beta)(e^x - 1)}. \tag{59}$$

This is correct in the limiting cases $x = 0$, $\alpha_A = \alpha_B$, α_A/β and α_B/β large, and α_A/β and α_B/β small. This is also a "Goldman" equation.

D. At Most One Ion per Channel

This is a case in which, for some reason (e.g., ionic repulsion), a channel can accommodate only one ion at a time. The flux, when $x = 0$, is given by equation 17 of reference 16.

A solution for arbitrary x and n is not difficult. The steady-state linear equations are

$$\begin{aligned} 0 &= (\alpha_A p^0 - \beta p_0) + (\kappa_B p_1 - \kappa_A p_0), \\ 0 &= (\kappa_A p_0 - \kappa_B p_1) + (\kappa_B p_2 - \kappa_A p_1), \end{aligned} \tag{60}$$

etc., where $p^0 = 1 - p_0 - p_1 - \cdots - p_n$ (probability channel is empty). The diagram method (7) is useful in this case. After considerable algebra, we find

$$\frac{J}{M} = \frac{\beta(\alpha_A e^x - \alpha_B)}{\sum} = \frac{p^0(x)(\alpha_A e^x - \alpha_B)}{e^x + 1 + [\beta(e^x - 1)/(\kappa_A - \kappa_B)]}, \tag{61}$$

where

$$\begin{aligned} \sum = (\alpha_A + \alpha_B)\left(\frac{\kappa_B - \kappa_A e^x}{\kappa_B - \kappa_A}\right) + \beta(1 + e^x) + \beta^2\left(\frac{1 - e^x}{\kappa_B - \kappa_A}\right) \\ + \frac{\beta\alpha_A[n\kappa_A e^x - (n + 1)\kappa_B e^x + \kappa_B]}{(\kappa_B - \kappa_A)^2} + \frac{\beta\alpha_B[n\kappa_B - (n + 1)\kappa_A + \kappa_A e^x]}{(\kappa_B - \kappa_A)^2}. \end{aligned} \tag{62}$$

The Parlin-Eyring method (15) readily gives the second form of equation 61 (compare equation 33) but this method does not provide $p^0(x)$. When n is large,

$$\frac{J}{M} = \frac{\kappa x^2(\alpha_A e^x - \alpha_B)}{n^2[\alpha_A(xe^x + 1 - e^x) - \alpha_B(1 + x - e^x)]}. \tag{63}$$

This does not have the form of a "Goldman equation." Note that β is absent. Two special cases of equation 63 are:

$$x = 0: J/M = 2\kappa(\alpha_A - \alpha_B)/n^2(\alpha_A + \alpha_B), \tag{64}$$

$$\alpha_A = \alpha_B: J/M = (\kappa x/n)(1/n);\ p(N) = 1/n;\ p^0 = \beta/n\alpha. \tag{65}$$

E. Arbitrary $f(N)$; Almost Empty Channel

We have restricted ourselves so far in this section to the linear electrostatic potential shown in Fig. 25. We now extend this work somewhat. We consider an arbitrary variation in potential as in Fig. 26.

The top curve in the figure shows the variation of the electrostatic potential through the membrane, starting from zero outside (B) and ending at ψ (or $x = \epsilon\psi/kT$) inside (A). This electrostatic potential curve is assumed to be unperturbed by M^+ ions in the channel. The binding potential is U as in Fig. 25. There are $n + 1$ equivalent binding sites in a channel, and we take n to be a large number (here and in section 6 F). The electrostatic potential at site N is $\psi f(N, x)$, which defines $f(N, x)$. Above, we examined the special case $f(N, x) = 1 - (N/n)$ (Fig. 25), which leads to the Goldman equation. This not only assumes a "constant field" (linear electrostatic potential), but also does not allow for Donnan effects at the edges of the membrane.

Incidentally, it is easy to treat a generalized U in Fig. 26 such that sites 0 and n are different from the rest (e.g., 0 and n are protein sites; $1, 2, \cdots, n - 1$ are lipid sites).

When $\psi = 0$, the adsorption and desorption rate constants (for sites 0 and n) are α_A, α_B, and $\beta_A = \beta_B = \beta$. We assume that the "jump" constants (Fig. 26) are

$$\kappa_{AN} = \kappa \exp\left\{-\frac{[f(N+1) - f(N)]x}{2}\right\},$$

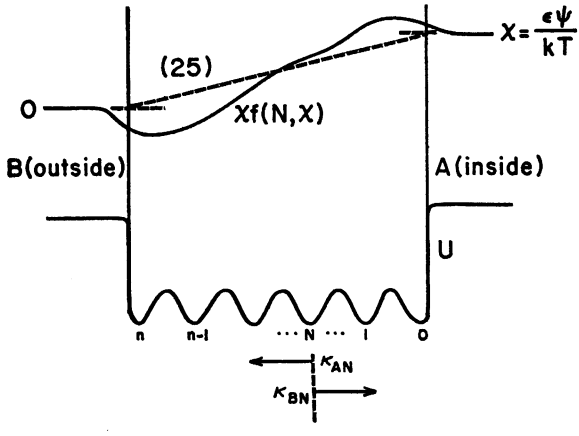

FIGURE 26 Multisite ionic transport model. Arbitrary variation of electrostatic potential. Line labeled (25) as in Fig. 25.

and

$$\kappa_{BN} = \kappa \exp\left\{\frac{[f(N) - f(N-1)]x}{2}\right\}. \tag{66}$$

Let $p_N \ll 1$ be the steady-state probability that the Nth site is occupied. Then the steady-state linear equations are

$$\begin{aligned} 0 &= (\alpha_A' - \beta' p_0) + (\kappa_{B1} p_1 - \kappa_{A0} p_0), \\ 0 &= (\kappa_{A0} p_0 - \kappa_{B1} p_1) + (\kappa_{B2} p_2 - \kappa_{A1} p_1), \end{aligned} \tag{67}$$

etc. The steady-state flux $(A \rightarrow B)$ is

$$J/M = \alpha_A' - \beta' p_0 = \kappa_{A0} p_0 - \kappa_{B1} p_1 = \cdots. \tag{68}$$

The primes indicate that these rate constants are x-dependent in accordance with

$$p_0 = \frac{\alpha_A'}{\beta'} = \frac{\alpha_A}{\beta} e^{(1-f_0)x} \quad \text{and} \quad p_n = \frac{\alpha_B'}{\beta''} = \frac{\alpha_B}{\beta} e^{-f_n x}, \tag{69}$$

where $f_N \equiv f(N, x)$. It is not necessary explicitly to "split" the (thermodynamic) x factors between α_A (or α_B) and β.

With n large, we can treat N as a continuous variable. We then find from equations 66 and 67 that $p(N, x)$ satisfies the differential equation

$$\frac{\partial^2 p}{\partial N^2} + x \frac{\partial f}{\partial N} \frac{\partial p}{\partial N} + px \frac{\partial^2 f}{\partial N^2} = 0, \tag{70}$$

where $f(N, x)$ is considered to be a known function. Equation 36 is a special case $[f = 1 - (N/n)]$. Equations 69 provide the boundary conditions $[p(0, x)$ and $p(n, x)]$. A first integration of equation 70 gives

$$\frac{\partial p}{\partial N} + px \frac{\partial f}{\partial N} = c_1. \tag{71}$$

Then

$$p(N, x) = e^{-xf(N,x)}\left[c_2 + c_1 \int_0^N e^{xf(N',x)}\, dN'\right], \tag{72}$$

where, using equation 69,

$$c_1 = \frac{\alpha_B - \alpha_A e^x}{\beta \int_0^n e^{xf}\, dN} \quad \text{and} \quad c_2 = \frac{\alpha_A}{\beta} e^x. \tag{73}$$

The flux follows from equation 68:

$$\frac{J}{M} = -\kappa \frac{\partial p}{\partial N} - \kappa p x \frac{\partial f}{\partial N} = -\kappa c_1 = \frac{\kappa(\alpha_A e^z - \alpha_B)}{\beta \int_0^n e^{zf}\, dN}. \tag{74}$$

As a check, we have also derived equation 74 by the Parlin-Eyring (15) method (n large). Equations 70 and 74 are of the Nernst-Planck type.

Equation 74 is a generalization of the Goldman equation. Clearly, J is not usually a linear function of x when $\alpha_A = \alpha_B$ (i.e., $M_e^+ = M_i^+$). In fact, even with an arbitrary constant field, $J(x)$ is not linear (when $\alpha_A = \alpha_B$). For suppose

$$f(0, x) = 1 + a(x), \quad f(n, x) = b(x),$$
$$f(N, x) = (1 + a) - (1 + a - b)(N/n). \tag{75}$$

Above, in this section, we took $a = b = 0$. Then, from equation 74,

$$\frac{J}{M} = \frac{\kappa x(1 + a - b)(\alpha_A e^z - \alpha_B)}{\beta n[e^{(1+a)x} - e^{bx}]}. \tag{76}$$

This is not linear in $x(\alpha_A = \alpha_B)$ even when $a = b$ (except $a = b = 0$) or $a = -b$. It would, of course, be approximately linear if $a(x)$ and $b(x)$ are always small compared to x.

The function $p(N, x)$ in equation 72 is generally not simple. Exceptions (in addition to cases above) are: (a) equilibrium ($c_1 = 0$); and (b) $\alpha_A = \alpha_B$, linear f, and $a = b$, in which case $p(N, x) = (\alpha/\beta)e^{-ax}$ (independent of N).

F. Arbitrary $f(N)$; Channel with Arbitrary Density

This problem is not difficult in principle, with n large and $f(N, x)$ arbitrary, but numerical calculations are a bit involved. We merely write down the general equations here. Proceeding as in section 6 C, we find the differential equation

$$\frac{\partial^2 p}{\partial N^2} + x \frac{\partial f}{\partial N} \frac{\partial p}{\partial N}(1 - 2p) + p(1 - p)x \frac{\partial^2 f}{\partial N^2} = 0, \tag{77}$$

which is a generalization of equations 51 and 70. A first integration gives

$$\frac{\partial p}{\partial N} + x \frac{\partial f}{\partial N} p(1 - p) = c_1. \tag{78}$$

This is a so-called Riccati equation. The flux is again found to be $J/M = -\kappa c_1$. The boundary conditions are

$$p_0 = \frac{\alpha_A e^{(1-f_0)x}}{\alpha_A + \beta} \quad \text{and} \quad p_n = \frac{\alpha_B e^{-f_n x}}{\alpha_B + \beta}. \tag{79}$$

Finally, we note that, in all of these cases (n large), $p(N, x)$ does not depend on κ, and that J is simply proportional to κ.

This research was supported in part by research grants from the National Science Foundation and the General Medical Sciences Institute of the U.S. Public Health Service.

Received for publication 11 August 1970 and in revised form 13 May 1971.

REFERENCES

1. HILL, T. L., and Y. CHEN. 1970. *Proc. Nat. Acad. Sci. U.S.A.* **65**:1069.
2. HILL, T. L., and Y. CHEN. 1970. *Proc. Nat. Acad. Sci. U.S.A.* **66**:189.
3. HILL, T. L., and Y. CHEN. 1970. *Proc. Nat. Acad. Sci. U.S.A.* **66**:607.
4. TASAKI, I. 1968. Nerve Excitation. Charles C. Thomas, Publisher, Springfield, Ill.
5. ADAM, G. 1968. *Z. Naturforsch.* **23b**:181.
6. BLUMENTHAL, R., J.-P. CHANGEUX, and R. LEFEVER. 1970. *J. Membrane Biol.* **2**:351.
7. HILL, T. L. 1968. Thermodynamics for Chemists and Biologists. Addison-Wesley Publishing Co., Inc., Reading, Mass. 141–153.
8. HILL, T. L. 1966. *Proc. Nat. Acad. Sci. U.S.A.* **55**:1379.
9. MOZHAYEVA, G. N. 1969. *Biophysics.* **14**:68.
10. GOLDMAN, D. E. 1943. *J. Gen. Physiol.* **27**:37.
11. PLONSEY, R. 1969. Bioelectric Phenomena. McGraw-Hill Book Company, New York. 112–115.
12. GORDON, R. 1970. *J. Appl. Probab.* **7**:373.
13. HILL, T. L. 1964. Thermodynamics of Small Systems, Part II. W. A. Benjamin, Inc., New York. xi.
14. HILL, T. L. 1966. *Proc. Nat. Acad. Sci. U.S.A.* **56**:840, 844.
15. PARLIN, R. B., and H. EYRING. 1954. *In* Ion Transport Across Membranes. H. T. Clarke, editor, Academic Press, Inc., New York. 105.
16. HILL, T. L., and O. KEDEM. 1966. *J. Theor. Biol.* **10**:399.